Photodissociation of Bis(*S*-benzyl-1,2-diphenyl-1,2-ethylenedithiolato)metal (Ni, Pd, Pt) Complexes

Shin-ichi Ohkoshi, Yasunori Ohba, Masamoto Iwaizumi, and Seigo Yamauchi*

Institute for Chemical Reaction Science, Tohoku University, Katahira, Sendai 980-77, Japan

Miharu Ohkoshi-Ohtani, Keiichi Tokuhisa, Masatsugu Kajitani, Takeo Akiyama, and Akira Sugimori*

Department of Chemistry, Faculty of Science and Technology, Sophia University, Kioi-cho 7-1, Chiyoda-ku, Tokyo 102, Japan

Received September 25, 1995[⊗]

Bis(*S*-benzyl-1,2-diphenyl-1,2-ethylenedithiolato)metal (Ni,Pd,Pt) (**1a**−**c**) complexes are known to undergo photochemical reactions that produce the corresponding neutral free metal dithiolene $M(S_2C_2Ph_2)_2$ (**3a**−**c**) complexes in solution. The reaction mechanisms of these photoreactions were examined by means of EPR and UV/vis absorption techniques. In the first step of the reaction the photodissociation of a C−S bond occurs to yield one benzyl radical and the monobenzyl dithiolene complex radical (**2a**−**c**). Both radicals were observed by time-resolved electron paramagnetic resonance (TREPR). The benzyl radical was also trapped by TEMPO (2,2,6,6-tetramethylpiperidine-1-oxyl). Analysis of the TREPR signals shows that the radicals are produced from the excited triplet states of **1a**−**c** within 100 ns. From the analyses of time-resolved and steady state EPR data, and absorption spectra, the intermediate complex radicals (**2a**−**c**) were assigned as $[M(S_2C_2Ph_2)\{S_2(CH_2Ph)C_2Ph_2\}]$ (M = Ni, Pd, Pt). Spin densities on the central metals were determined from their anisotropic *g* values and hyperfine coupling constants by comparing the data with those of $[M(S_2C_2Ph_2)_2]^-$. A correlation between the spin density and the decay time of the intermediate complexes (**2a**−**c**) was pointed out. The second step of the reaction was found to be the dissociation of a second benzyl substituent, which occurs in the dark. The reaction rate was discussed in terms of the spin density (ρ_M) on the metal and the S−C(benzyl) bond order $(\rho_s\rho_c)^{1/2}$ of the intermediate radicals, **2a**−**c**.

1. Introduction

Various kinds of studies on metal dithiolato and dithiolene complexes have been reported in the literature.[1] Recently, metal dithiolato complexes have been introduced as electron acceptors in molecular superconductors.[2] The dithiolato ligand is considered to be an "noninnocent" ligand which exhibits two stable forms: a dithiolato anion form (reduced) and a neutral dithiolene form (oxidized) depending on the medium.

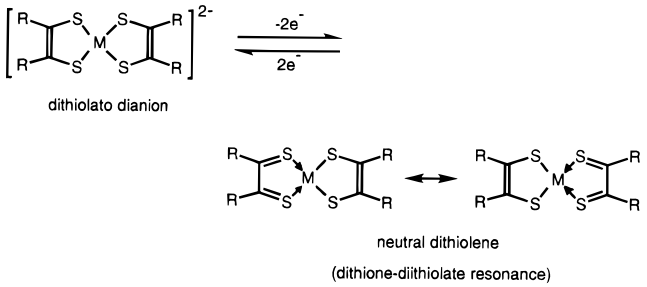

The neutral bis(1,2-diphenyl-1,2-ethylenedithiolato)metal complexes $[M(S_2C_2Ph_2)_2]$ undergo reactions mainly at the sulfur atoms. They react with norbornadiene and quadricyclane to give an adduct in which norbornene-5,6-diyl bridges two sulfur atoms, for example. This adduct can be photochemically dissociated to regenerate the neutral dithiolene metal complexes and norbornadiene.[3,4]

Schrauzer et al. first reported syntheses and photoreactions of bis(*S*-benzyl-1,2-diphenyl-1,2-ethylenedithiolato)metal (Ni, Pd, Pt) (**1a**−**c**) complexes.[5,6] From the results of the X-ray structural analyses, it was found that the MS_4 moieties of **1a**−**c** are planar. These complexes have no dithione−dithiolate resonance properties and in view of the spectral similarity of **1a** and $[Ni(S_2C_2Ph_2]^{2-}$, they can be reasonably formulated as "classical" complexes containing M(II). When **1a**−**c** were irradiated by visible light, the neutral bis(1,2-diphenyl-1,2-ethylenedithiolato)metal complexes (**3a**−**c**), $M(S_2C_2Ph_2)_2$, and dibenzyl were produced. Although the photoreactions were likely to occur in a stepwise fashion

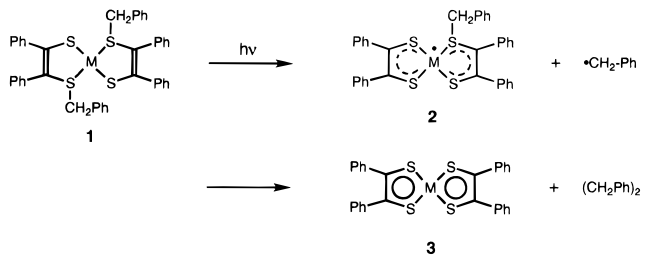

as postulated by Schrauzer and Rabinowitz,[5] details of these reactions have not been reported so far.

* To whom correspondence should be addressed.

[⊗] Abstract published in *Advance ACS Abstracts,* July 1, 1996.

(1) Reviews: (a) Schrauzer, G. N. *Acc. Chem. Res.* **1969**, *2*, 72. (b) McCleverty, J. A. *Prog. Inorg. Chem.* **1969**, *10*, 49. (c) Burns, R. P.; Mcauliffe, C. A. *Adv. Inorg. Chem. Radiochem.* **1979**, *22*, 303. (d) Mueller-Westerhoff, U. T.; Vance, B. Dithiolene and Related Species. In *Comprehensive Coordination Chemistry*; ed by Wilkinson, G. Gillard, R., McCleverty, J. A., Eds.; Pergamon Press: Oxford, England, 1987; Vol. 2, p 545. (e) Kisch, H. *Coord. Chem. Rev.* **1993**, *125*, 155.

S0020-1669(95)01235-3 CCC: $12.00

In a previous study, we carried out optical and EPR measurements in order to clarify mechanisms of the photodissociations of **1a**−**c**.[7] The experimental techniques included time-resolved EPR (TREPR), conversional steady state EPR, transient UV−vis absorption and their simultaneous observations. A free-radical trapping experiment was also made by TEMPO. We reported the photodissociation of **1a**,[7] which occurs *via* the excited triplet state of **1a**, producing the benzyl radical and the intermediate metal complex radical, **2a**. The observed complex radical has a lifetime on the order of 10^3 s. Such a long-life radical complex is unusual, and it seemed very interesting to us to study its electronic structure.

In this paper we report the results of the photodissociations of complexes having a homologous series of metals, Pd (**1b**) and Pt (**1c**). We also discuss the electronic structures of the intermediate complexes radicals. UV−vis absorption, TREPR and steady state EPR spectra were observed and analyzed for this purpose. We have determined spin densities and lifetimes of the intermediate radicals. The rate of the second step of the dissociation reaction is discussed in terms of the electronic structures of intermediate complex radicals including effects of the metal and the benzyl substituents, $-NO_2$ (**1a$_1$**) and $-OCH_3$ (**1a$_2$**).

2. Experimental Section

2.1. Preparation of Complexes. **Ni{S$_2$(CH$_2$Ph)$_2$C$_2$Ph$_2$)$_2$ (1a) and Its Derivatives (1a$_1$, 1a$_2$).** To a suspension of 5 g of Ni($S_2C_2Ph_2)_2$-(**3a**) in 75 mL of methanol were added 2.5 mL of 50% (wt) NaOH solution and 0.375 g of $NaBH_4$, heating at 50 °C for 1 h to accomplish the reaction of the complex to the dianion. To this solution was added 3.50 g of benzyl bromide, and orange crystals of the benzyl derivative precipitated after stirring overnight. The reaction mixture was filtered, giving 3.34 g of the product (45% yield). Purification by flash chromatography using a Wako silica gel C-300 column with benzene as eluent afforded the pure crystal.

Ni{$S_2(CH_2C_6H_5NO_2)C_2Ph_2\}_2$ (**1a$_1$**) (23% crude yield) and Ni{$S_2(CH_2C_6H_5OCH_3)C_2Ph_2\}_2$ (**1a$_2$**) (42% crude yield) were prepared by the same procedure except that 4-nitrobenzyl bromide and 4-methoxybenzyl bromide were used, respectively. Analysis data for **1a$_1$**: ^{1}H NMR ($CDCl_3$), $\delta = 8.11$ ppm (4H, d, $J = 8.78$ Hz), 7.54 ppm (4H, d, $J = 8.79$ Hz), 6.97−7.21 ppm (20H, m), 4.07 ppm (4H, s); electronic absorption/benzene, λ_{max} (ϵ) = 330 nm (12 000), 360 nm (18 000); GC−MS (70 eV) *m/z* 514 (M^+). Data for **1a$_2$**: ^{1}H NMR ($CDCl_3$), $\delta = 7.30$ ppm (4H, d, $J = 8.79$ Hz), 7.12 ppm (4H, d, $J = 8.79$ Hz), 6.96−7.22 ppm (20H, m), 3.97 ppm (4H, s), 3.79 ppm (6H, s); electronic absorption/benzene, λ_{max} (ϵ) = 354 nm (26 800), 390 nm (17 000); GC−MS, *m/z* 484 (M^+).

Pd{S$_2$(CH$_2$Ph)C$_2$Ph$_2\}_2$ (1b) and Pt{(S$_2$C$_2$Ph$_2$)C$_2$Ph$_2\}_2$ (1c). The same method was applied for the syntheses of **1b** and **1c**, which were also purified by flash chromatography with a Wako silica gel FC-40 column using *n*-hexane/CH_2Cl_2 as the eluent mixture. We obtained red brown **1b** (30% crude yield) and orange **1c** (60% crude yield) crystals.

2.2. Measurements. UV−Vis Absorption Spectra. The samples **1a**−**c** were dissolved in benzene ($(5-10) \times 10^{-5}$ mol dm^{-3}) and placed in a 10 mm quartz cell. After deaeration with a flow of Ar for 15 min, they were irradiated with a 500 W Xe lamp ($\lambda > 360$ nm). On irradiation, the original solutions turned green, brown, and purple for **1a**, **1b**, and **1c**, respectively.

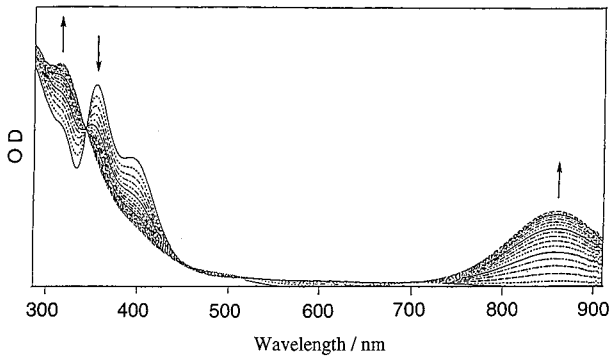

Figure 1. UV−vis spectral changes of **1a** (1×10^{-4} mol dm^{-3}) in a benzene solution during the irradiation with a Xe lamp ($\lambda > 360$ nm). The spectra were observed every 2 minutes.

TREPR Spectroscopy. The deaerated solution (ca. 1×10^{-3} mol dm^{-3}) flowing through the EPR cavity at ca. 2 mL/min was excited by a Lamda Physik LPX 100i excimer laser at 308 nm. TREPR spectra were observed without field modulation by an NF BX-531 digital boxcar integrator. The details of the TREPR apparatus and experimental procedure have been reported elsewhere.[8]

Steady State EPR Spectroscopy. Steady state EPR spectra were observed with a JEOL RE 3X X-band EPR spectrometer. EPR spectra of the photochemically produced species were observed at room temperature in the EPR cell by flowing the solution at ca. 3 mL/min (M = Ni) or 12 mL/min (M = Pt). The spectra at 77 K were obtained for the solid solutions (1×10^{-3} mol dm^{-3} in benzene), which were frozen rapidly by liquid nitrogen immediately after the irradiation with a 1 kW Xe lamp ($\lambda > 360$ nm) at room temperature.

Simultaneous Observations of UV−Vis Absorption and EPR Spectra. Transient UV−vis absorption spectra were observed in the EPR cavity by using a Photal MCPD-1000 rapid scan spectrometer. EPR spectra were observed as described above. A 1 kW Xe lamp was used as a light source.

Radical Trapping by TEMPO. A dilute solution of complex **1a** and the radical scavenger TEMPO(2,2,6,6-tetramethylpiperidine-1-oxyl) in benzene was irradiated with a 500 W Xe lamp ($\lambda > 360$ nm). The product of TEMPO-CH_2Ph was detected by NMR.[9]

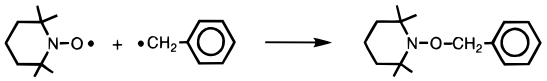

3. Results

3.1. UV−Vis Absorption Spectra. UV−vis absorption spectra of **1a** in benzene were pursued after an irradiation with the high pressure mercury lamp as shown in Figure 1. The final spectrum of the irradiated solution was identical with that of [Ni($S_2C_2Ph_2$)] (**3a**). The spectra for Pd (**1b**) and Pt (**1c**) complexes also showed similar behavior.

3.2. Time-Resolved EPR Spectra. The TREPR spectrum of **1a** in benzene solution was observed at 1 μs after the laser excitation as shown in Figure 2. Two kinds of radicals were observed and assigned as the benzyl radical ($g = 2.0021$) and the intermediate complex radical **2a** ($g = 2.042$) in the previous paper.[7] In the case of **1b** (Figure 2b) two EPR signals were also observed and assigned as the benzyl radical and the complex radical ($g = 2.014$) **2b** by referring to **2a** and the steady state EPR spectrum (Section 3.3). In the case of **1c**, only the benzyl radical was observed by TREPR (Figure 2c). For the substituted benzyl derivatives, 4-nitro (**1a$_1$**) and 4-methoxy (**1a$_2$**), the radicals of the corresponding benzyl derivatives and the

(2) (a) Brossard, L.; Ribault, M.; Valade, L.; Cassoux, P. *Physica B ± C (Amsterdam)* **1986**, *143*, 378. (b) Kobayashi, H.; Bun, K.; Naito, T.; Kato, R.; Kobayashi, A. *Chem. Lett.* **1991**, 2163.
(3) Schrauzer, G. N.; Mayweg, V. P. *Am. Chem. Soc.* **1965**, *87*, 1483.
(4) Kajitani, M.; Kohara, M.; Kitayama, T.; Akiyama, T.; Sugimori, A. *J. Phys. Org. Chem.* **1989**, *2*, 32.
(5) Schrauzer, G. N.; Rabinowiz, H. N. *J. Am. Chem. Soc.* **1968**, *90*, 4297.
(6) Zhang, C.; Reddy, H. K.; Schlemper, E. O.; Schrauzer, G. N. *Inorg. Chem.* **1990**, *29*, 4100.
(7) Ohtani, M.; Ohkoshi, S.; Kajitani, M.; Akiyama, T.; Sugimori, A.; Yamauchi, S.; Ohba, Y.; Iwaizumi, M. *Inorg. Chem.* **1992**, *31*, 3873.
(8) Yamauchi, S.; Hirota, N. *J. Phy* s. *Chem.* **1984**, *88*, 4631.
(9) TEMPO−CH_2Ph: ^{1}H NMR ($CDCl_3$) $\delta = 1.18$ (6H, m, CH_2), 1.29 (12H, s, CH_3), 4.90 (2H, s, CH_2 at benzyl), and 6.75−7.52 ppm (6H, m, Ph); GC−MS (70 eV) *m/z* 156 ($M^+ - CH_2Ph$) and 91 ($M^+ -$ TEMPO).

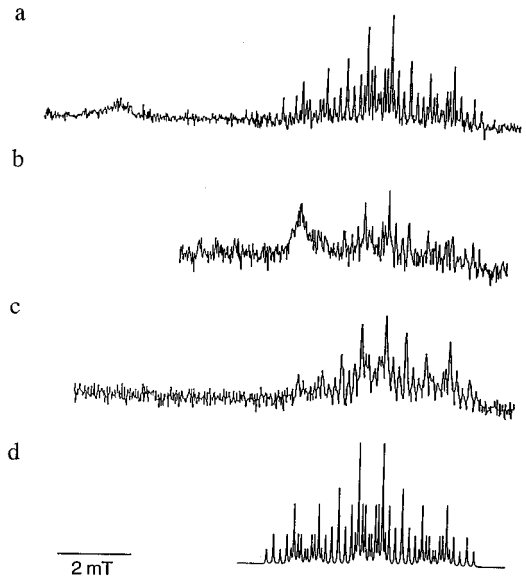

Figure 2. Time-resolved EPR spectra observed at 1 μs for the photolysis of (a) **1a**, (b) **1b**, and (c) **1c** in benzene at room temperature. Part d shows the simulated spectrum of the benzyl radical with the EPR parameters reported in ref 7.

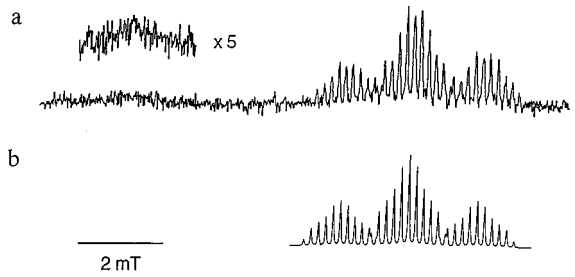

Figure 3. Time-resolved EPR spectrum observed for the photolysis of $\mathbf{1a_1}$ under the same conditions described in Figure 2. The spectrum of the 4-nitrobenzyl radical was simulated by the EPR parameters summarized in ref 10.

complex radicals ($g = 2.041$ and 2.043) were observed (Figure 3a) and assigned in the same manner. The simulation of the 4-nitrobenzyl radical is shown in Figure 3b.[10]

All the observed spectra showed net absorptive (A) polarizations. The spectra of the benzyl radical in the systems of **1a** and its derivatives ($\mathbf{1a_1}$, $\mathbf{1a_2}$) were nearly symmetric to the center of the spectra. However, in the cases of **1b** and **1c** the intensities at higher magnetic fields were slightly stronger than those at lower fields, which is described as an E/A* pattern. Here E and A* denote an emission and an enhanced absorption of the microwave, respectively.

3.3. Steady State EPR Spectra. The steady state EPR spectrum having $g = 2.042$ was observed at room temperature for **1a** in benzene, Figure 4a. In the case of **1b**, the intermediate radical **2b** ($g = 2.014$) showed six lines due to hyperfine coupling (hfc) on ^{105}Pd ($I = {}^5/_2$, natural abundance 22.2%), Figure 4b. In the case of **1c**, the formed radical **2c** ($g = 2.026$) showed doublet lines due to hfc of ^{195}Pt ($I = {}^1/_2$, natural abundance 33.7%), Figure 4c. **2a** was assigned as the complex radical from the similarity of the EPR parameters of $[Ni(S_2C_2Ph_2)]^-$ as reported previously.[7] Now from the similarities of the EPR spectra of **2a**, **2b**, and **2c**, radicals **2b** and **2c** are assigned to the complex radicals $[M(S_2C_2Ph_2)\{S_2(CH_2Ph)\text{-}C_2Ph_2\}]^\bullet$, M = Pd and Pt, respectively, which are produced by release of one of the two benzyl substituents from the parent complexes (**1b** and **1c**).

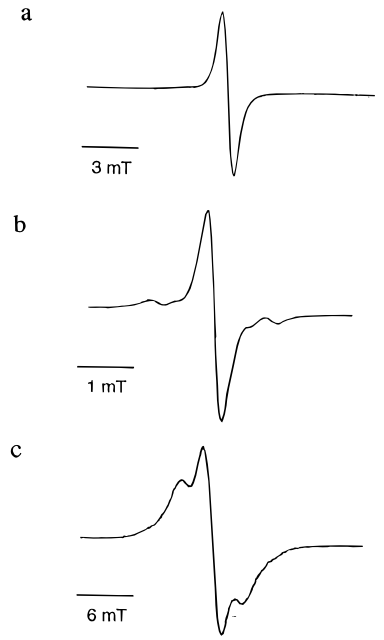

Figure 4. Steady state EPR spectra observed for the photolysis of (a) **1a**, (b) **1b**, and (c) **1c** at room temperature in benzene.

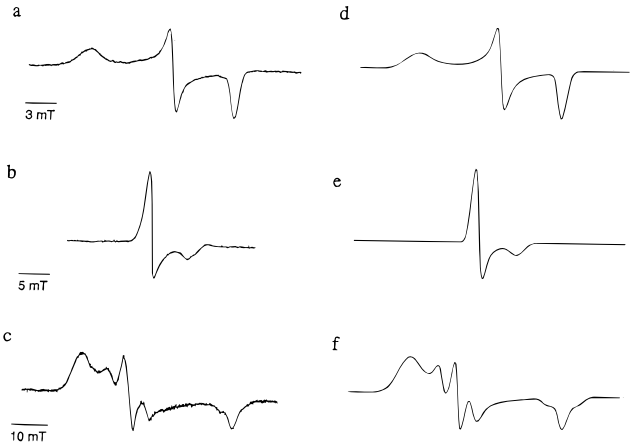

Figure 5. Steady state EPR spectra observed at 77K after the photolysis of (a) **1a**, (b) **1b**, and (c) **1c** at room temperatures in benzene and their simulations (d−f) with the EPR parameters summarized in Table 1.

These spectra are temperature dependent, reflecting a difference in an extent of averaging in anisotropies of the g factor and hyperfine coupling constant (hfcc). The spectra of **2a**−**c** observed at 77 K are shown in Figure 5a−c and were analyzed by simulation with the EPR parameters summarized in Table 1. The complex radical having the largest anisotropy of the g factor is **2c** ($g = 2.121-1.898$) and the radical having the smallest anisotropy is **2b** ($g = 2.033-1.988$). The hyperfine structure of Pt was observed and analyzed. For the Pd complex, the hyperfine splitting was not resolved due to its broader line width. The benzyl radical was not detected by steady state EPR neither at room temperature nor at 77 K in all systems.

3.4. Simultaneous Observations of Transient Absorption and EPR Spectra. The steady state EPR signals and the UV−vis absorptions of the intermediate species were observed at the same time. The decay of the EPR signal of **2a** was analogous to the rise of the UV−vis absorption of **3a** ($\lambda_{max} = 857$ nm) as described previously.[7] Within the time-resolution

(10) The EPR parameters of the 4-nitrobenzyl radical are summarized: $g = 2.0021$ and hfcc's at the CH_2, NO_2, ortho, and meta protons of the phenyl ring are 14.8×10^{-4}, 4.8×10^{-4}, 1.6×10^{-4}, and 1.6×10^{-4} cm^{-1}, respectively.

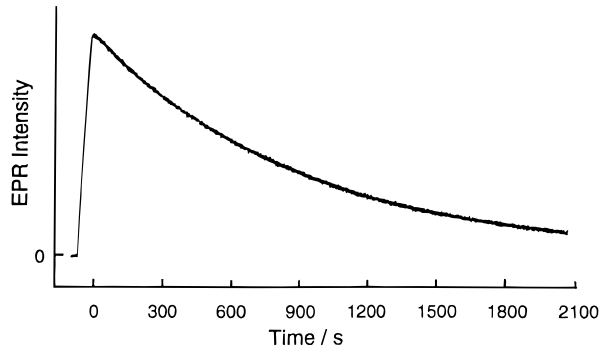

Figure 6. Decay curve observed at the central peak of the steady state EPR signal in the **1c** system at room temperature.

of our apparatus (~100 ms), the absorption at $\lambda_{max} = 890$ nm appeared and then gradually decreased with a concurrent appearance of **3a**. Therefore, the absorption at $\lambda_{max} = 890$ nm was assigned to that of **2a** (Figure 7a). In the cases of the photodissociations of **1b** and **1c**, the absorption spectra of **2b** and **2c** were also observed as shown in parts b and c of Figure 7. The decays of the **2a**−**c** signals followed single-exponential functions under weak irradiation and/or low concentrations of the samples. The obtained decay rate constants are summarized in Table 2.

4. Discussion

4.1. First Step of the Photodissociation. The photodissociations of **1a**−**c** in benzene solution occur via the C−S bond cleavage affording the benzyl radical and the complex radicals **2a**−**c**, which were observed simultaneously by TREPR. The benzyl radical was also observed by trapping with TEMPO. The observed TREPR spectrum of the benzyl radical in the **1a** system showed the polarization of a nearly symmetric absorptive (A) pattern. In the cases of the **1b** and **1c** systems, the TREPR spectra showed the E/A* (A + E/A) polarization. These polarizations are produced during the reaction due to CIDEP (chemically induced dynamic electron polarization).

There are two CIDEP mechanisms for the radical−radical interactions: TM (triplet mechanism)[11,12] and RPM (radical pair mechanism).[13,14] The TM polarization is generated from an anisotropy of intersystem crossing from the photo-excited singlet state to the triplet sublevels. The TREPR spectrum due to TM shows the symmetric net absorption (A) or net emission (E) of the microwave, indicating that a photoreaction occurs *via* the excited triplet state of the reactant molecule. The nearly symmetric absorptive TM signal observed for the **1a** system gives the conclusion that the photoreaction occurs *via* the excited triplet state.

On the other hand, the RPM polarization is due to the mixing between singlet and triplet radical pair states. The TREPR spectrum due to RPM shows the emission at the low magnetic field side and the absorption at the high field side giving an E/A pattern or just the reverse A/E pattern. The E/A and A/E patterns indicate that the photoreaction occurs *via* the excited triplet state and the excited singlet state, respectively for $J < 0$ (J, exchange integral) as the usual case. The TREPR spectra of the benzyl radical observed for systems of **1b** and **1c** are slightly distorted (E/A*), indicating involvement of the RPM polarization (E/A), though the dominant absorptive (A) TM polarizations are also observed for these systems. From both the TM (A) and RPM (E/A) polarizations we concluded that the photoreactions of **1b** and **1c** also occur *via* the excited triplet states. We considered the reason why the TREPR spectra involved the RPM polarization for **1b** and **1c** as being due to the decrease of the TM contribution. The TM polarization is quenched either by fast electron spin−lattice relaxations due to heavier metals or by slow reactions in the **1b** and **1c** systems.[11,12] For **1c** the former is preferred because the TREPR signal of the benzyl radical was similarly observed as in other systems.

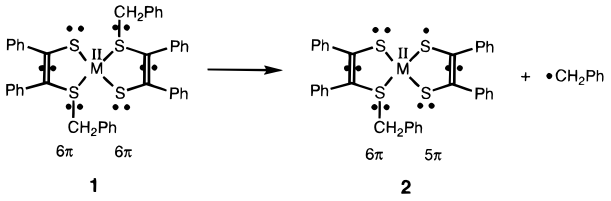

4.2. Second Step of the Photodissociation. In photochemical reactions of organometallic complexes, lifetimes of the intermediate radicals are generally short ($<10^{-3}$ s). However, in our case the intermediate radicals **2a**−**c** have long lifetimes with an order of 10^3 s at room temperature. We discuss the electronic structures of **2a**−**c** in relation to their stabilities and reactivities.

As expected from the syntheses and electronic structures of **1a**−**c**, their UV−vis spectra resemble those of the dianions of **3a**−**c**. The photodissociations of **1a**−**c** occur by homolysis to generate the benzyl radical and the complex radicals **2a**−**c**, and then the spectra of **2a**−**c** and of the monoanions should be similar also. Several theoretical studies have been reported for the metal dithiolato complexes. In 1965 Schrauzer and Mayweg first assigned HOMO's of $[Ni(S_2C_2Ph_2)_2]^{2-}$ and $[Ni(S_2C_2Ph_2)_2]^{-}$ as the b_{3g} orbital on the basis of the MO calculation using a semiempirical Hückel approximation.[3] Sano et al. confirmed this result with the DV−Xα MO calculation.[15] The b_{3g} orbital is constructed by the d_{yz} orbital of the central metal and the p_z orbitals of the sulfur and carbon atoms. In the b_{3g} orbital, the Ni−S and S−C bonds are antibonding in nature, while the C−C bond is bonding. A removal of one electron from the b_{3g} orbital makes the Ni−S and S−C bonds stronger while weakening the C−C bond. Therefore, the ligand character of the $[Ni(S_2C_2Ph_2)_2]^{-}$ is situated between those of a dithiolato type, $[Ni(S_2C_2Ph_2)_2]^{2-}$, and the dithiolene type, $[Ni(S_2C_2Ph_2)_2]$. On the basis of these analyses the unpaired electron in $[Ni(S_2C_2Ph_2)_2]^{-}$ is considered to be delocalized over the entire complex:

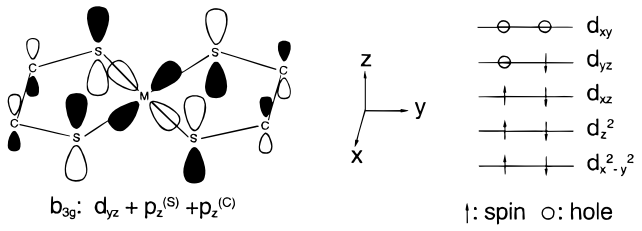

Schrauzer and Mayweg assigned the very intense near-infrared bands in the spectra of $Ni(S_2C_2H_2)_2$(720nm) and $[Ni(S_2C_2H_2)_2]^{-}$ (870 nm) to $\pi-\pi^*$ transitions, $2b_{1u} \rightarrow 3b_{3g}$.[3] This red shift in the $\pi-\pi^*$ transition of $[Ni(S_2C_2H_2)_2]^{-}$ was rationalized by the calculation and the experiment.[3] These near-infrared bands were also observed in the transient absorption spectra of **2a** (890 nm),

(11) Wong, S. K.; Hutchinson, D. A.; Wan, J. K. S. *Chem. Phys.* **1973**, *58*, 985.
(12) Pedersen, J. B.; Freed, J. H. *J. Chem. Phys.* **1975**, *62*, 1706.
(13) Adrian, F. *J. Chem. Phys.* **1971**, *54*, 3918.
(14) Tominaga, K.; Yamauchi, S.; Hirota, N. *J. Chem. Phys.* **1989**, *88*, 533.
(15) Sano, M.; Adachi, H.; Yamatera, H. *Bull. Chem. Soc. Jpn.* **1981**, *53*, 2636.

Table 1. EPR Parameters[a] of **2a**−**c**, $[M(S_2C_2Ph_2)_2]^-$, and $[M(mnt)_2]^-$ (M = Ni, Pd, Pt) Complexes

complexes	g	g_x	g_y	g_z	A	A_x	A_y	A_z	$A_{\|\|}^S$	A^S
2a (M = Ni)	2.042	2.088	2.035	1.997						
2b (M = Pd)	2.014	2.033	2.027	1.988	3.8					
2c (M = Pt)	2.026	2.121	2.044	1.898	−48	−17.8	−70.2	−53.2		
$[Ni(S_2C_2Ph_2)_2]^-$ [b]	2.052	2.119	2.043	2.000						
$[Pd(S_2C_2Ph_2)_2]^-$ [b]	2.022	2.051	2.041	1.960	6.9	9.2	6.6	5.0		
$[Pt(S_2C_2Ph_2)_2]^-$ [b]	2.039	2.169	2.065	1.845	−75	−32	−109	−84		
$[Ni(mnt)_2]^-$ [c]	2.065	2.156	2.042	1.996	4.4	14.0	−5.3	4.4	14.4	4.6
$[Pd(mnt)_2]^-$ [c]	2.023	2.071	2.043	1.956	7.2	10.3	5.9	5.4	16.8	5.8
$[Pt(mnt)_2]^-$ [c]	2.037	2.245	2.065	1.827	−74.9	0.0	−125.5	−99.1	16.3	

[a] Hyperfine coupling constants are in 10^{-4} cm^{-1}. [b] Reference 18. [c] Reference 22.

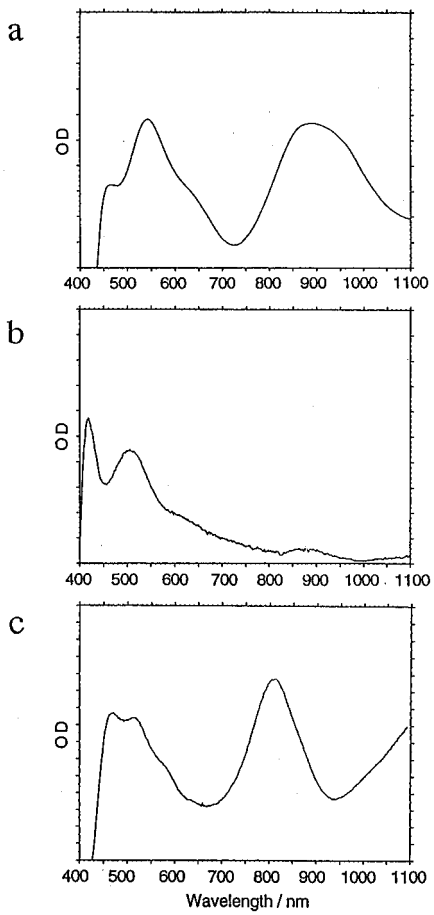

Figure 7. Transient UV−vis absorption spectra observed after irradiation of (a) **1a**, (b) **1b**, and (c) **1c** at room temperature.

Table 2. Spin Density on the Central Metal and Decay Rate Constant of **2a**−**c**

	ρ_M	$k/10^{-4}$ s^{-1}	$\tau/10^3$ s^a
2a (M = Ni)	0.19	6.7	1.5
2a$_1$		7.5	1.3
2a$_2$		5.5	1.8
2b (M = Pd)	0.06	2.0	5.0
2c (M = Pt)	0.23	8.3	1.2

[a] $\tau = 1/k$.

2b (880 nm), and **2c** (810 nm)[16] (Figure 7), which confirms our assignments of **2a**−**c**.

Maki et al. have first observed the EPR spectrum of $[Ni\{S_2C_2(CN)_2\}_2]^-$ in the mixed crystal and determined the ground state configuration of the metal ion as $Ni^{3+}(d_{xy}^2 d_{yz}; d^7)$ by analyzing the g factor and the hfcc of ^{61}Ni.[17] Later on they also confirmed the delocalized nature of the b_{3g} orbital that was proposed by Schrauzer and Mayweg[3] from the analysis of the hfcc of the ^{33}S atoms.[18]

The EPR spectra of **2a**−**c** and the monoanions showed qualitatively similar patterns;[19,20] the observed anisotropies in g, $\Delta g_{ii} = g_{ii} - g_e$; $i = x, y, z$), of **2a**−**c** closely resembled those of $[M(S_2C_2Ph_2)_2]^-$ (M = Ni, Pd, Pt) (Table 1). In the case of **2c**, the anisotropic g factors and the hyperfine coupling constants of Pt were ca. 70% of those of $[Pt(S_2C_2Ph_2)_2]^-$. From these results, we assigned the electronic structures of **2a**−**c** as the b_{3g} type and considered that only the spin distributions are a little different from those of the monoanions, $[M(S_2C_2Ph_2)_2]^-$. The ligands of **1a**−**c** and **3a**−**c** were of the dithiolato type and the dithiolene type, respectively. From a comparison of the results of the monoanions, the ligand types of **2a**−**c** are considered to be a mixture of the dithiolato and dithiolene types. Such an unique electronic structure of the dithiolato−dithiolene resonance type (insert) may explain the long lifetimes of **2a**−**c**.

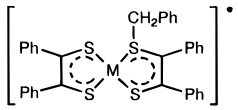

2a-c

The spin density on the central metals of **2a**−**c** was estimated from the anisotropic part of the g factor Δg_{ii} by comparing our values with the reported values for the monoanions. The central metal and sulfur atoms contribute to the anisotropic g factors mainly as $\Delta g_{ii}^{(M)}$ and $\Delta g_{ii}^{(S)}$ because the spin-orbit coupling constants of these atoms, ζ_{Ni}=685 cm^{-1}, ζ_S=352 cm^{-1}, are much larger than that of the carbon atom, ζ_c = 29 cm^{-1}. In this case the $\Delta g_{zz}^{(S)}$ is very small, because $\Delta_{gzz}^{(S)} \propto \langle p_i^{(S)}|l_z^{(S)}|p_z^{(S)}\rangle = 0$ ($i = x, y, z$). Consequently, the g factors of **2a**−**c** are described as follows, allowing the estimation of the spin densities at M from the Δg_{zz} values.

$$\Delta g_{xx} = \Delta g_{xx}^{(M)} + \Delta g_{xx}^{(S)} \quad (1a)$$

$$\Delta g_{yy} = \Delta g_{yy}^{(M)} + \Delta g_{yy}^{(S)} \quad (1b)$$

$$\Delta g_{zz} = \Delta g_{zz}^{(M)} \quad (1c)$$

The spin densities (ρ_M) of the $[M(mnt)_2]^-$ (mnt = maleonitriledithiolato) (M = Ni, Pd, Pt) complex monoanions have been reported, and as shown in Table 1 the EPR properties, average g value (g) and isotropic hfcc (A), are nearly the same between $[M(mnt)_2]^-$ and $[M(S_2C_2Ph_2)]^-$. Therefore, the ρ_M's of

(16) The absorption coefficient of **2b** at 880 nm is smaller than those of the corresponding bands of **2a** and **2b** by a factor of ca. 5.

(17) Maki, A. H.; Edelstein, N.; Davison, A.; Holm, R. H. *J. Am. Chem. Soc.* **1964**, *86*, 4580.
(18) Schmitt, R. D.; Maki, A. H. *J. Am. Chem. Soc.* **1968**, *90*, 2288.

$[M(mnt)_2]^-$ were used as the reference densities for the calculation of ρ's in **2a**−**c**. For $[Ni(mnt)_2]^-$ and $Pd[(mnt)_2]^-$ the spin densities were obtained as 0.24 (0.19) at Ni(Pd), and 0.50 (0.56) at four S atoms[21] from the EPR analyses. The MO calculation supported these values as 0.18 (Ni) and 0.64 (four S′).[15] For $[Pt(mnt)_2]^-$ the spin density at Pt was calculated as 0.39 by using the obtained hfcc's (Table 1)[22] and Maki's method.[17,23] We estimated the spin densities (ρ_M) at the central metals (Ni, Pd, Pt) of **2a**−**c** from these values (0.24, 0.19, 0.39) of $[M(mnt)_2]^-$ and the obtained ratios (0.8, 0.30, 0.59) of Δg_{zz} as 0.19, 0.06, and 0.23, respectively as summarized in Table 2. The remaining 77−94% of the unpaired electrons in **2a**−**c** are considered to be delocalized over the ligands.

From the results of the first order decays of **2a**−**c** and the decay−rise relations[7] observed for **2a**−**c** and **3a**−**c**, we concluded that the observed decay is dominated by the dissociation of **2a**−**c**. The reaction rates for the second step k_2, were obtained as 6.7×10^{-4}, 2.0×10^{-4} and 8.3×10^{-4} s^{-1} for **2a**, **2b**, and **2c**, respectively. Here we found the correlation between k_2 and ρ_M such that the larger ρ_M is the larger k_2 is. We explain this relation in terms of the orbital character of the S atoms. The MS_4 moieties of **1a**−**c** were planar as indicated by the X-ray structural analysis and the bonding orbitals of the S atom having the $S-CH_2Ph$ bond were nearly sp^3 in nature.[6] The hybrid character at the S atoms of **2a**−**c** is situated between sp^3 and sp^2 hybridizations due to the dithiolato−dithiolene resonance. The increase of the spin density at the central metal (M) causes the decrease of the corresponding spin densities at the S atoms because the d_{yz} orbital of M interacts strongly with the p_z orbitals of S in the b_{3g} orbital. The decrease of the p_z density at S diminishes the bonding character in the $S-CH_2Ph$ bond. Then the correlation between $\rho_M(d_{yz})$ and the second dissociation rate could be rationalized.

The fact that the second dissociation is controlled by the spin density (ρ_s) of the S(−CH_2Ph) atom is also tested by the spin density (ρ_c) of the other side atom, C(−S) in the benzyl substituent. As shown in Table 2, the electron-withdrawing nitro (**2a$_1$**) and donating methoxy (**2a$_2$**) benzyl derivatives provide the larger and the smaller dissociation rates, respectively, when compared with the parent benzyl complex radical (**2a**). This clearly indicates that a smaller ρ_c makes the dissociation faster and confirms the correlation among k_2, ρ_S, and ρ_M.

5. Conclusion

We have presented direct evidences for the dissociation of the benzyl radical in the first step of the photochemical reactions of bis(*S*-benzyl-1,2-diphenyl-1,2-ethylenedithiolato)metal (Ni, Pd, Pt) complexes (**1a**−**c**). The photoreactions occur from the excited triplet states of **1a**−**c** within an order of 100 ns. Stable intermediate metal complex radicals (**2a**−**c**) were observed and characterized by EPR and transient absorption techniques. The unique change of the ligand character from a dithiolato type to a dithiolato−dithiolene resonance type was suggested as a possible source for stabilities of the intermediate radicals, **2a**−**c**.

These complex radicals were decomposed in the dark to the corresponding dithiolene metal complexes (**3a**−**c**) on a time scale of 1000 s. The spin density on the central metal and the dissociation rate of **2a**−**c** were determined and their correlations were analyzed in terms of orbital natures at the metal (Ni, Pd, Pt) and the $S-CH_2Ph$ bond.

Acknowledgment. This work was supported by Grant-in Aid for Scientific Research on Priority Area "Molecular Magnetism" (Area Nos. 228/04242102 and 04242202) from the Ministry of Education, Science, and Culture, Japan.

IC951235S

(19) Bowmaker, G.; Boyd, P. D. W.; Campbell, G. K. *Inorg. Chem.* **1983**, *22*, 1208.
(20) Geiger, Jr. W. E.; Allen, C. S.; Mines, T. G.; Senftleber, F. C. *Inorg. Chem.* **1977**, *16*, 2003.
(21) The spin densities at the sulfur atoms were estimated by the following equations, where the hfcc ($A^{(S)}$) were reported by Kirmse et al.[22] $A_{||}^{(S)} = a + 2T$, $A_{\perp}^{(S)} = a - T$, $T = (A_{||}^{(S)} - A_{\perp}^{(S)})/3$. Here $A_{||}^{(S)}$ and $A_{\perp}^{(S)}$ are parallel and perpendicular parts of the hfcc at the sulfur atoms, and a and T are isotropic and anisotropic parts, respectively.
(22) (a) Kirmse, R.; Stach, J.; Dietzsch, W.; Steimecke, G.; Hoyer, E. *Inorg. Chem.* **1980**, *19*, 2679. (b) Kirmse, R.; Dietzsch, W. *J. Inorg. Nucl. Chem.* **1976**, *38*, 255. (c) Kirmse, R.; Stach, J.; Dietzsch, W.; Solov'ev, B. V. *J. Inorg. Nucl. Chem.* **1977**, *39*, 1157.
(23) Heuer, W. B.; True, A. E.; Swepston, P. N. Hoffman, B. M. *Inorg. Chem.* **1988**, *27*, 1474.